Jurnal Teknologi

Full Paper

ROBUST HOVERING CONTROLLER FOR UNCERTAIN MULTIROTOR MICRO AERIAL VEHICLES (MAVS) IN GPS-DENIED ENVIRONMENTS: IMAGE-BASED

Dafizal Derawi[a,b], Nurul Dayana Salim[a,b], Hairi Zamzuri[a,*], Mohd Azizi Abdul Rahman[a], Kenzo Nonami[c]

[a]Malaysia-Japan International Institute of Technology, Universiti Teknologi Malaysia, Kuala Lumpur, Malaysia
[b]Mechatronic Systems Laboratory, Robotic Systems Enterprise, Melaka, Malaysia
[c]Faculty of Engineering, Chiba University, Chiba, Japan

Article history
Received
1 November 2015
Received in revised form
21 March 2016
Accepted
23 March 2016

*Corresponding author
hairi.kl@utm.my

Graphical abstract

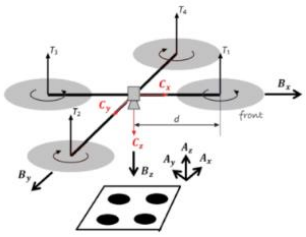

Abstract

This paper proposes an image-based robust hovering controller for multirotor micro aerial vehicles (MAVs) in GPS-denied environments. The proposed controller is robust against the effects of multiple uncertainties in angular dynamics of vehicle which contain external disturbances, nonlinear dynamics, coupling, and parametric uncertainties. Based on visual features extracted from the image, the proposed controller is capable of controlling the pose (position and orientation) of the multirotor relative to the fixed-target. The proposed controller scheme consists of two parts: a spherical image-based visual servoing (IBVS) and a robust flight controller for velocity and attitude control loops. A robust compensator based on a second order robust filter is utilized in the robust flight control design to improve the robustness of the multirotor when subject to multiple uncertainties. Compared to other methods, the proposed method is robust against multiple uncertainties and does not need to keep the features in the field of view. The simulation results prove the effectiveness and robustness of the proposed controller.

Keywords: Image-based; robust control; hovering; multirotor micro aerial vehicles

1.0 INTRODUCTION

Multirotor micro aerial vehicles (MAVs) are widely used for many monitoring and surveillance tasks, in both indoor and outdoor environments. They are highly manoeuvrable, able to fly at low altitude, and are easier to control than traditional helicopter. Quadrotor platform has become the universal testbed for aerial robotic researches and a standard platform for multirotor MAV. It consists of four rotors attached to a rigid body frame and has the ability to do vertical take-off and landing (VTOL).

Over the last decades, different advanced control schemes have been developed for aerial vehicles. Vision-based control (usually known as visual servoing) is also one of the popular methods that have been extensively developed for aerial vehicles in order to increase the flexibility and accuracy of aerial robot system. The task in vision-based control is to control the pose (position and orientation) of aerial vehicles relative to the target by using visual features extracted from the image. There are two main categories: image-based and position-based control systems. In position-based visual servo (PBVS), the error is computed in the 3D Cartesian space where the pose of the target with respect to camera frame are estimated based on a geometric model of the target, a calibrated camera, and visual features. On the other hand, in image-based

visual servo (IBVS), the error is determined in the 2D image plane by controlling the task directly from the image plane (no pose estimation of the target). By defining the control task directly within the image coordinate space, the controller is inherently robust to camera calibration and alleviates the requirement for a 3D model of the target [1].

Position control with respect to fixed targets by using image features is a popular application for helicopters capable of hovering or near hovering flight [2]-[4]. However, their methods require a very accurate model of the target and is very difficult to obtain when it deals with dynamics system. For observing fixed targets from a fixed-wing aircraft, hovering task is not possible since it has to maintain the forward velocity for lifting and usually, they will do circular orbits using IBVS technique [5]-[7]. Automated landing of fixed-wing aircraft has also been a popular application of IBVS control, utilizing a desired view of runway features to achieve control during each phase of landing [7]-[11]. However, the effects of multiple uncertainties in vehicle dynamics were not addressed in previous studies. In addition, previous research which relied on IBVS has difficulty in keeping the target features in field of view.

In this paper, the proposed image-based robust controller is capable of controlling the pose (position and orientation) of the multirotor MAV with respect to fixed-target points without the GPS and it relies on visual features extracted from the image only. The proposed controller consists of two parts: the spherical image-based visual servoing (IBVS) controller and the robust flight controller based on robust compensating technique [12]. The camera model is an "eye-in-hand" type configuration, where a downward facing camera is attached to the centre of the airframe of the multirotor MAV. The dynamic of the system is modelled to determine the dynamic responses of the camera signals based on general assumptions about the structure of the environment. The simulation results prove the effectiveness and robustness of the proposed controller and show high potential for practical applications.

This paper is different compared to previous works since it proposes an image-based robust hovering control for multirotor MAVs which considers the influence of multiple uncertainties in angular dynamics of vehicle and utilizes a new method of spherical imaging technique for camera model introduced in [13]. As a result, multirotor MAVs are robust against uncertainties such as disturbances, nonlinear dynamics, coupling, and parametric uncertainties and does not require keeping target features in the field of view.

The rest of this paper is arranged as follows. Section 2 describes the system overview. Section 3 presents the proposed image-based robust hovering control scheme for the multirotor MAV. Section 4 presents the simulation results and finally, Section 5 summarizes this paper and provides suggestion for future research.

2.0 SYSTEM

2.1 Model of Multirotor Micro Aerial Vehicle

As mentioned earlier, the quadrotor platform has become a universal testbed for aerial robotic researches and the standard platform of multirotor MAVs. Thus, the rigid body dynamics of the quadrotor is described in this section. The quadrotor consists of four rotors attached to a body frame as shown in Figure 1.

Let us define $\{A\} = \{A_x, A_y, A_z\}$ as an inertial frame, $\{B\} = \{B_x, B_y, B_z\}$ denote a body-fixed frame for the quadrotor airframe, $\{C\} = \{C_x, C_y, C_z\}$ denote a camera-fixed frame. As can be seen, the camera and body-fixed frames have their positive z-axis downward following the standard aerospace convention. The camera is fixed and centred at the centre of gravity (CoG) of $\{B\}$. Let us denote $\xi = (\xi_x \quad \xi_y \quad \xi_z)^T \in \{A\}$ as the position of the origin of the body-fixed frame $\{B\}$ with respect to inertial frame $\{A\}$ and $\eta = (\phi \quad \theta \quad \psi)^T \in \{B\}$ as the attitude vector of roll ϕ, pitch θ, and yaw ψ angles. The rigid body dynamics model can be derived by the Euler-Lagrange approach as [14]

$$\begin{aligned} \ddot{\xi}_x &= -(\sin\phi\sin\psi + \cos\phi\sin\theta\cos\psi)T/m \\ \ddot{\xi}_y &= -(\cos\phi\sin\theta\sin\psi - \sin\phi\cos\psi)T/m \\ \ddot{\xi}_z &= g - (\cos\phi\cos\theta)T/m \end{aligned} \tag{1}$$

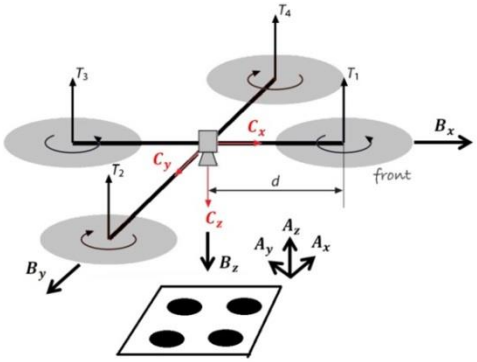

Figure 1 Notation for the quadrotor in hovering control task

$$\begin{aligned} \ddot{\phi} &= I_\phi{}^{-1} C_\phi(\eta,\dot{\eta})\dot{\eta} + I_\phi{}^{-1}(\tau_\phi + w_\phi) \\ \ddot{\theta} &= I_\theta{}^{-1} C_\theta(\eta,\dot{\eta})\dot{\eta} + I_\theta{}^{-1}(\tau_\theta + w_\theta) \\ \ddot{\psi} &= I_\psi{}^{-1} C_\psi(\eta,\dot{\eta})\dot{\eta} + I_\psi{}^{-1}(\tau_\psi + w_\psi) \end{aligned} \tag{2}$$

where $C_i(\eta,\dot{\eta})$ $(i = \phi,\theta,\psi)$ is the Coriolis term [14], T is the total thrust force, m is the total mass of vehicle, g is the gravity constant, τ_i $(i = \phi,\theta,\psi)$ is the torque applied to the airframe by aerodynamics of rotors, w_i $(i = \phi,\theta,\psi)$ is the external disturbance, and I_i $(i = \phi,\theta,\psi)$ is the moments of inertia. Actually, (1) and (2) describe the translational and rotational motions of the vehicle, respectively.

The thrust force T_i $(i = 1,2,3,4)$ is produced by single rotor in the air and can be modelled as [15]

$$T_i = b\omega_i{}^2 \tag{3}$$

where b denotes the thrust constant which satisfies $b > 0$ and ω_i is the angular velocity of the rotor. The total upward thrust is

$$T = \sum_{i=1}^{4} T_i \tag{4}$$

The torque τ_i $(i = \phi, \theta, \psi)$ about each axis of body frame could be written as

$$\begin{aligned} \tau_\phi &= d(T_4 - T_2) \\ \tau_\theta &= d(T_1 - T_3) \\ \tau_\psi &= k_{fm}(T_1 - T_2 + T_3 - T_4) \end{aligned} \tag{5}$$

where d is the distance between the centre of mass and the rotor, k_{fm} denotes the positive force-to-torque scaling factor in aerodynamics of rotor.

From (4), the control input of thrust u_T could be defined as

$$u_T = {\omega_1}^2 + {\omega_2}^2 + {\omega_3}^2 + {\omega_4}^2 \tag{6}$$

From (5), the attitude control input for roll u_ϕ, pitch u_θ, and yaw u_ψ could be defined as

$$\begin{aligned} u_\phi &= {\omega_4}^2 - {\omega_2}^2 \\ u_\theta &= {\omega_1}^2 - {\omega_3}^2 \\ u_\psi &= {\omega_1}^2 - {\omega_2}^2 + {\omega_3}^2 - {\omega_4}^2 \end{aligned} \tag{7}$$

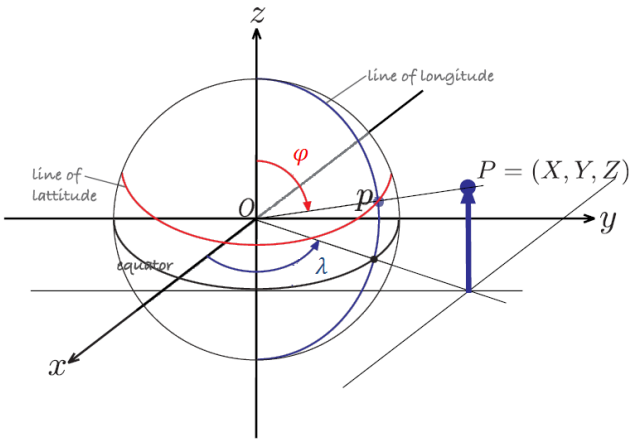

Figure 2 The coordinate system. P is mapped to p on the sphere represented by colatitude φ and longitude λ.

From (5) and (7), the attitude control input for roll, pitch, and yaw angles are proportional to torque, such that $\tau_i = a_{i1}u_i$ where $a_{\phi 1} = db$, $a_{\theta 1} = db$, and $a_{\psi 1} = k_{fm}b$.

In practice, the control inputs will be distributed to each motor by using a power distribution board and thus, the control inputs can be controlled directly to control the motions of the vehicle.

Let us define the vehicle parameter constant $a_i = {I_i}^{-1}a_{i1}$ $(i = \phi, \theta, \psi)$ and it consists of nominal N and uncertain Δ values, such that

$$a_i = {a_i}^N + {a_i}^\Delta, \quad i = \phi, \theta, \psi$$

Assumption 1: The uncertain part ${a_i}^\Delta$ are bounded. The nominal part ${a_i}^N > 0$ and satisfies $|{a_i}^N - a_i| < {a_i}^N$. Let us define the positive constant ρ_i $(i = \phi, \theta, \psi)$ as $\rho_i = |{a_i}^N - a_i|/{a_i}^N$. Therefore, ρ_i satisfy that $0 \le \rho_i < 1$.

Assumption 2: The total upward thrust is bounded with $T \ge \delta_T$ where $\delta_T > 0$.

Assumption 3: The pitch and roll angles satisfy that $\theta \in (-\pi/2 + \delta_\theta, \pi/2 - \delta_\theta)$ and $\phi \in (-\pi/2 + \delta_\phi, \pi/2 - \delta_\phi)$ where $\delta_i > 0$ $(i = \theta, \phi)$.

Assumption 4: The external disturbance w_i $(i = \phi, \theta, \psi)$ is bounded.

Assumption 5: The attitude angles have the desired reference signal as i_d $(i = \phi, \theta, \psi)$. The reference signals and their derivatives ${i_d}^{(k)}$ $(i = \theta, \phi, \psi; k = 0,1,2)$ are piecewise uniformly bounded.

Assumption 6: The effects of uncertainties in translational motion (1) are very small in hovering conditions. Thus, the effects of uncertainties in (1) can be ignored. If the angular dynamics (rotational motion) of the multirotor MAV is robust, then the whole flight controller is robust in hovering conditions.

2.2 Image Jacobian for Spherical Camera

The catadioptric camera and fisheye lens camera are popular types of non-perspective cameras in literature. Because of that, many different projection models and image Jacobians were developed in literature. One alternative is that the features from any type of camera can be projected to sphere as shown in Figure 2.

The image Jacobian is derived using the similar method that has been used for perspective camera. Let us consider the camera is moving with velocity $v = (v_x, v_y, v_z)^T$ and angular velocity $\omega = (\omega_x, \omega_y, \omega_z)^T$ and it is observing a world point P in the world frame. $P = (X, Y, Z)$ denotes the point with camera relative coordinates and the velocity of the point relative to the camera frame can be described as

$$\dot{P} = -\omega \times P - v \tag{8}$$

From (8), it can be derived as

$$\begin{aligned} \dot{X} &= Y\omega_z - Z\omega_y - v_x \\ \dot{Y} &= Z\omega_x - X\omega_z - v_y \\ \dot{Z} &= X\omega_y - Y\omega_x - v_z \end{aligned} \tag{9}$$

As can be seen in Figure 2, P can be projected to point $p = (x, y, z)$ on the sphere's surface centred at the origin

$$x = \frac{X}{R}, \qquad y = \frac{Y}{R}, \qquad z = \frac{Z}{R} \tag{10}$$

where R is the distance between the world point and camera origin with $R = \sqrt{(X^2 + Y^2 + Z^2)}$

The spherical points satisfy that $x^2 + y^2 + z^2 = 1$ where one of the Cartesian coordinates is redundant. The angle of colatitude φ is defined by using minimal spherical coordinate system as shown in the following equation

$$\varphi = \sin^{-1} r, \qquad \varphi \in [0, \pi) \tag{11}$$

where $r = \sqrt{x^2 + y^2}$. The azimuth angle (longitude) is

$$\lambda = \tan^{-1}\frac{y}{x}, \qquad \lambda \in [-\pi, \pi) \tag{12}$$

The Cartesian coordinates for the point feature $p = (\varphi, \lambda)$ are

$$x = r\cos\lambda, \qquad y = r\sin\lambda, \qquad z = cos\varphi \tag{13}$$

where $r = \sin\varphi$. From (9)-(13), the following equation can be obtained

$$\begin{aligned} X &= R\sin\varphi\, cos\lambda \\ Y &= R\sin\varphi\sin\lambda \\ Z &= R\cos\varphi \end{aligned} \tag{14}$$

Finally, the spherical optical flow equation in the matrix form can be derived as

$$\begin{pmatrix}\dot{\varphi}\\ \dot{\lambda}\end{pmatrix} = J(\varphi,\lambda,R)\begin{pmatrix}v_x\\ v_y\\ v_z\\ \omega_x\\ \omega_y\\ \omega_z\end{pmatrix} \quad (15)$$

where the image feature Jacobian $J(\varphi,\lambda,R)$ is

$$J = \begin{pmatrix} -\frac{c\lambda c\varphi}{R} & -\frac{s\lambda c\varphi}{R} & \frac{s\varphi}{R} & s\lambda & -c\lambda & 0 \\ \frac{s\lambda}{Rs\varphi} & -\frac{c\lambda}{Rs\varphi} & 0 & \frac{c\lambda c\varphi}{s\varphi} & \frac{s\lambda c\varphi}{s\varphi} & -1 \end{pmatrix} \quad (16)$$

where c and s denote cosine and sine, respectively.

3.0 ROBUST HOVERING CONTROLLER: IMAGE-BASED

In this section, the task in robust hovering control is to control the pose of the multirotor MAV in hovering conditions relative to fixed targets (points) under the effects of uncertainties in the angular dynamics of vehicle by using visual features extracted from the image. The proposed control method does not require the state estimation of the target in Cartesian space and represents the task in terms of image error. The proposed method is particularly effective in situations where state estimation is difficult (e.g. GPS-denied environment). The overall proposed control deign is illustrated in Fig. 3.

Compared to the standard multirotor MAV control system:

1. The position errors for ξ_i $(i = x, y)$ in the proposed control design is given in the camera frame $\{C\}$ (same with body-fixed frame $\{B\}$), rather than inertial frame $\{A\}$.
2. The horizontal position ξ_i $(i = x, y)$, altitude ξ_z, and yaw angle ψ loops are no longer required in the proposed controller since the spherical IBVS controller generates the required velocities for multirotor motions.

3.1 Spherical IBVS Control

The normal step of computing a 2×6 Jacobian in (16) for each N feature points will result in

$$v = \begin{pmatrix}J_1\\ \vdots\\ J_N\end{pmatrix}^{-1}\begin{pmatrix}\dot{\varphi}_1\\ \dot{\lambda}_1\\ \vdots\\ \dot{\varphi}_N\\ \dot{\lambda}_N\end{pmatrix} \quad (17)$$

For $N > 3$ the camera motion can be solved by using the pseudo-inverse

$$v = J^{+}\dot{p}^{*} \quad (18)$$

where $\dot{p}^{*}$ denotes the desired velocity of the feature points in the $\lambda\varphi$ -space. The solution that reduces the norm of the feature velocity error is obtained by pseudo-inverse. Then, the point velocity is computed by a proportional controller as

$$\dot{p}^{*} = \alpha(p^{*} - p) \quad (19)$$

where p is the current feature point in $\lambda\varphi$ -space, p^{*} is the desired value of the feature point, and α denotes a gain which satisfies $\alpha > 0$.

As mentioned earlier, the camera frame $\{C\}$ is attached to the centre of the body frame $\{B\}$ and has similar positive direction of each axis. Therefore, the velocity of the camera is the same as the velocity of the multirotor MAV and thus, (17) can be written as

$$v_d = \alpha\begin{pmatrix}J_1\\ \vdots\\ J_N\end{pmatrix}^{+}(p^{*} - p) \quad (20)$$

$v_d = (v_x{}^{*} \quad v_y{}^{*} \quad v_z{}^{*} \quad \omega_z{}^{*})^T$ is the desired velocity of the multirotor MAV. It will be the reference signal of the robust flight control system. $\omega_x{}^{*}$ and $\omega_y{}^{*}$ are not needed in the robust flight control system since roll and pitch subsystems are controlled directly based on desired roll ϕ_d and pitch θ_d angles.

3.2 Robust Flight Control

The velocity control loop looks at the desired velocity of rigid body $(v_x{}^{*}, v_y{}^{*}, v_z{}^{*})$ produced by spherical IBVS control and compares that to the actual velocity of the multirotor MAV $(\dot{\xi}_x \quad \dot{\xi}_y \quad \dot{\xi}_z)$. In practice, the actual velocity can be estimated by using a commercial inertial navigation system or an observer. The desired roll ϕ_d and pitch θ_d angles are generated by the nominal velocity controller a

$$\phi_d = K_1^{\phi}\left(v_y{}^{*} - K_2^{\phi}\dot{\xi}_y\right) \quad (21)$$

$$\theta_d = K_1^{\theta}\left(v_x{}^{*} - K_2^{\theta}\dot{\xi}_x\right) \quad (22)$$

The altitude of the multirotor MAV ξ_z is controlled by

$$u_T = K_1^{T}\left(v_z{}^{*} - K_2^{T}\dot{\xi}_z\right) + \omega_0 \quad (23)$$

where K_1^{i} and K_2^{i} with $i = (\phi, \theta, T)$ are constant gains. ω_0 is the minimum rotor speed needed to produce a thrust equal to the weight of the aerial robot, that satisfies $\omega_0 = \sqrt{mg/4b}$.

For attitude control loop, let us define an angular error vector as $e_i = (e_{i1} \quad e_{i2} \quad e_{i3})^T$ $(i = \phi, \theta, \psi)$, where $e_{i1} = i_d - i$, $e_{i2} = \dot{e}_{i1}$, and $\dot{e}_{i3} = e_{i1}$.

Based on (2), let us define the error dynamical equations as

$$\dot{e}_i = A_i e_i + B_i(u_i + q_i), \quad i = \phi, \theta, \psi \quad (24)$$

Where

$$A_i = \begin{bmatrix}0 & 1 & 0\\ 0 & 0 & 0\\ 1 & 0 & 0\end{bmatrix}, \quad B_i = \begin{bmatrix}0\\ a_i{}^{N}\\ 0\end{bmatrix}$$

and q_i $(i = \phi, \theta, \psi)$ is the multiple uncertainties in angular dynamics of vehicle which consists of external disturbances, nonlinear dynamics, coupling, and parametric uncertainties with the following equation

$$q_i = \frac{I_i{}^{-1}C_i(\eta, \dot{\eta})\dot{\eta} + a_i{}^{\Delta}u_i + I_i{}^{-1}w_i - \ddot{r}_i}{a_i{}^{N}} \quad (25)$$

The attitude controller design for roll, pitch, and yaw subsystems contain a nominal linear controller and robust compensator. As can be seen in Figure 3, the attitude control input u_i $(i = \phi, \theta, \psi)$ is

$$u_i = u_i{}^{N} + u_i{}^{RC} \quad (26)$$

where $u_i{}^{N}(i = \phi, \theta, \psi)$ is the control input from a nominal linear controller and $u_i{}^{RC}(i = \phi, \theta, \psi)$ is the robust compensating signal from a robust compensator.

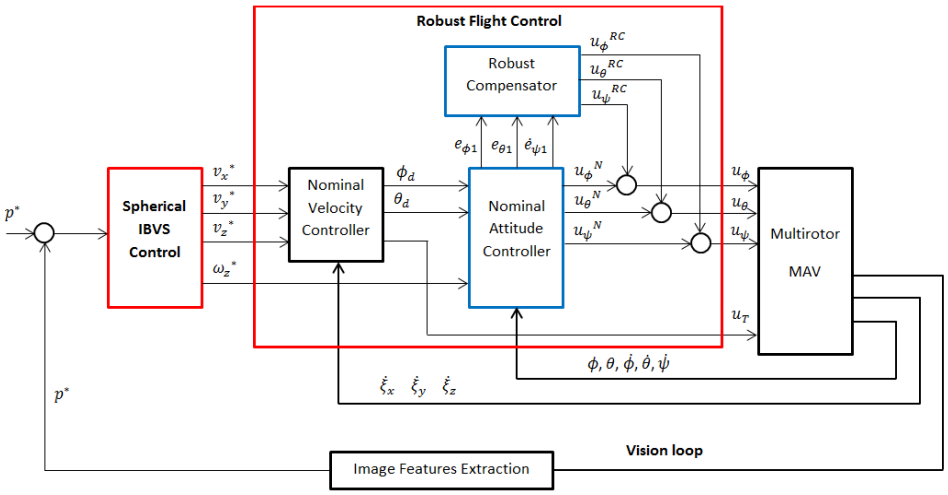

Figure 3 The overall block diagram of the proposed image-based robust hovering control of multirotor MAVs.

The nominal controller is designed based on proportional and derivative controllers to generate the nominal control input $u_i{}^N$ $(i = \phi, \theta)$

$$u_\phi{}^N = K_\phi^P(\phi_d - \phi) + K_\phi^D(\dot{\phi}_d - \dot{\phi}) \quad (27)$$

$$u_\theta{}^N = K_\theta^P(\theta_d - \theta) + K_\theta^D(\dot{\theta}_d - \dot{\theta}) \quad (28)$$

The terms $\dot{\phi}_d$ and $\dot{\theta}_d$ are commonly ignored since it is typically small. The gains K_i^P and K_i^D $(i = \phi, \theta)$ are determined by classical method based on an approximation of dynamic model and can be tuned to achieve excellent tracking performance of the nominal system.

The nominal control input for yaw subsystem $u_\psi{}^N$ is generated by

$$u_\psi{}^N = K_1^\psi\left(\omega_z{}^* - K_2^\psi\dot{\psi}\right) \quad (29)$$

where K_1^ψ and K_2^ψ are constant gains. The actual angular rate along B_z axis $\dot{\psi}$ can be obtained by gyroscopes.

The robust compensator is introduced to reduce the effects of the multiple uncertainties q_i $(i = \phi, \theta, \psi)$ in angular dynamics by computing the robust compensating signal as

$$u_i{}^{RC}(s) = -F_i(s)q_i(s), \quad i = \phi, \theta, \psi \quad (30)$$

where s is the Laplace operator and $F_i(s)$ $(i = \phi, \theta, \psi)$ is the robust filter, which forms the second order low pass filter

$$F_i(s) = \frac{f_{li}f_{si}}{(s + f_{li})(s + f_{si})}, \quad i = \phi, \theta, \psi$$

where f_{li} and f_{si} are parameters of the robust filter and must be larger than zero. The robust filter $F_i(s)$ $(i = \phi, \theta, \psi)$ has the property as described in [12]: if the parameters f_{li} and f_{si} $(i = \phi, \theta, \psi)$ are sufficiently large and satisfy that $f_{li} \gg f_{si} > 0$, the low pass filter $F_i(s)(i = \phi, \theta, \psi)$ has sufficiently wide frequency bandwidths. As a result, the low frequencies signal can pass through the filters. Therefore, $u_i{}^{RC} = -q_i$ since gains of the robust filter is approximate to one.

However, the multiple uncertainties q_i $(i = \phi, \theta, \psi)$ is unknown since it cannot be measured. Thus, from (24), the multiple uncertainties q_i $(i = \phi, \theta, \psi)$ is

$$q_i = \frac{\ddot{e}_{i1}}{a_i{}^N} - u_i \quad (31)$$

Then, from (30) and (31), $u_i{}^{RC}$ which do not depend on $q_i(s)$ can be derived mathematically in the following equation by introducing z_{1i} and z_{2i} as two new states of the robust filter

$$\dot{z}_{1i} = -f_{si}z_{1i} - f_{si}{}^2e_{i1} + a_i{}^Nu_i \quad (32)$$

$$\dot{z}_{2i} = -f_{li}z_{2i} + (f_{li} + f_{si})e_{i1} + z_{1i}$$

$$u_i{}^{RC} = -f_{li}f_{si}(e_{i1} - z_{2i})/a_i{}^N, \quad i = \phi, \theta, \psi$$

The robustness properties of the closed-loop control system are summarized by Theorem 1.

Theorem 1: If Assumptions 1-6 are met, the bounded initial state $e(0)$, for a specified constant ε, a finite-positive constant T^*, and sufficiently large parameters f_{li} and f_{si} $(i = \phi, \theta, \psi)$ satisfy that $f_{li} \gg f_{si} > 0$, then the state $e(t)$ is bounded to satisfy that $|e(t)| \leq \varepsilon, \forall t \geq T^*$.

Theorem 1 can be proven based on the small gain theory as presented in [16].

The robust compensator parameters f_{li} and f_{si} $(i = \phi, \theta, \psi)$ can be tuned by an on-line tuning procedure: set the values of f_{li} and f_{si} $(i = \phi, \theta, \psi)$ from a small one and increase these parameters which satisfy $f_{li} \gg f_{si} > 0$ until a satisfactory tracking performance is achieved [16].

4.0 SIMULATION RESULTS

Three different hovering cases have been considered. Firstly, the combination of the spherical IBVS and the nominal flight controller (velocity and attitude) is evaluated without the effects of multiple uncertainties. Then, the same controller is evaluated under the effects of multiple uncertainties. Finally, the proposed robust hovering controller is evaluated under the effects of multiple uncertainties. The vehicle parameters used in this section are taken from [15]. Simulation parameters for vision system are presented in Table 1. The flight controller parameters are presented in Table 2.

4.1 Case 1: Hovering Mission With The Nominal Controller Without The Effects Of Multiple Uncertainties

In this case, the multirotor MAV has to hover five meters above four target points without the effects of uncertainties by using the combination of the spherical IBVS and the nominal flight controller (velocity and attitude) without the robust compensator in the attitude loop. The multirotor MAV has initial position $\xi = (0 \quad 0 \quad 0)^T$. Figure 4 shows the corresponding responses. As can be seen, the feature points have smooth trajectory path in the $\lambda\varphi$ -space toward their desired position. Overall, the controller achieves good dynamical tracking performances for the nominal conditions.

4.2 Case 2: Hovering Mission With The Nominal Controller Under The Effects Of Multiple Uncertainties

The uncertainties are assumed as Gaussian noises with 250 mean and 1 variance values for q_θ only. q_ϕ and q_ψ are assumed to be 0. The same controller as Case 1 is considered. As can be seen in Figure 5, if the uncertainties are considered, the response of the nominal controller can no longer track the reference signal and its tracking errors become larger without boundaries. As a result, the multirotor MAV was not able to hover above four target points.

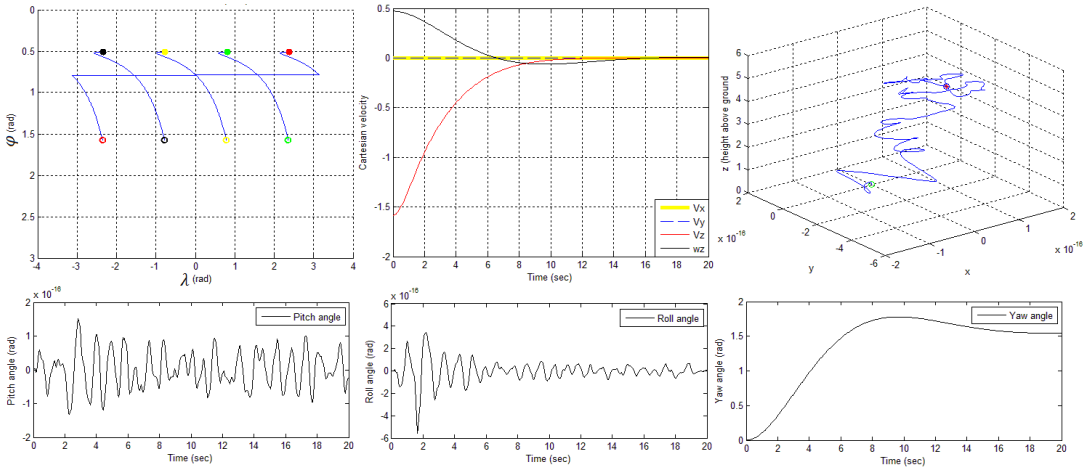

Figure 4 Case 1: a) The path of the point features in the $\lambda\varphi$ –space. "o" denotes initial position, "*" denotes the final position of features. b) Spatial velocity components. c) Vehicle/ camera position in Cartesian space. "o" denotes initial position, "*" denotes the final position of features. d) Attitude response for pitch, roll, and yaw angles. Note: The arrangement of figures is [a b c; d].

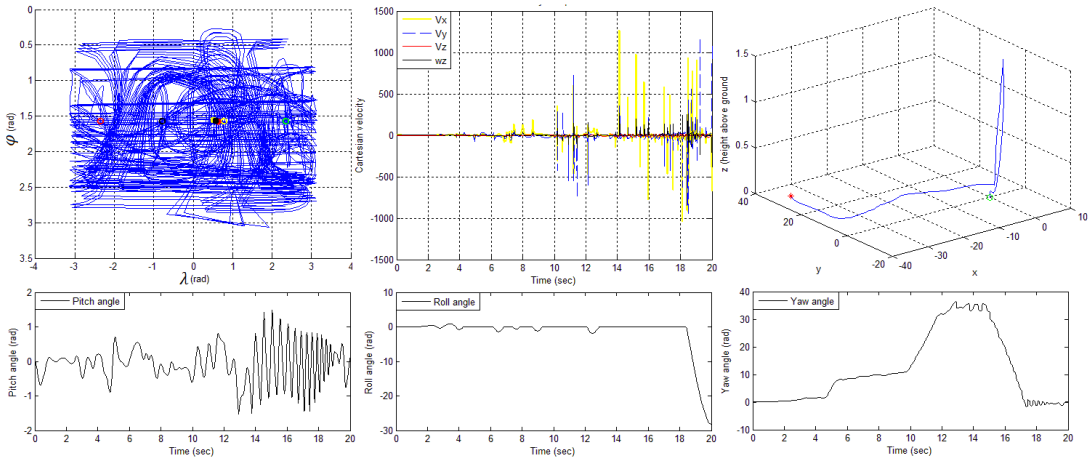

Figure 5 Case 2: a) The path of the point features in the $\lambda\varphi$ –space. "o" denotes initial position, "*" denotes the final position of features. b) Spatial velocity components. c) Vehicle/ camera position in Cartesian space. "o" denotes initial position, "*" denotes the final position of features. d) Attitude response for pitch, roll, and yaw angles. Note: The arrangement of figures is [a b c; d].

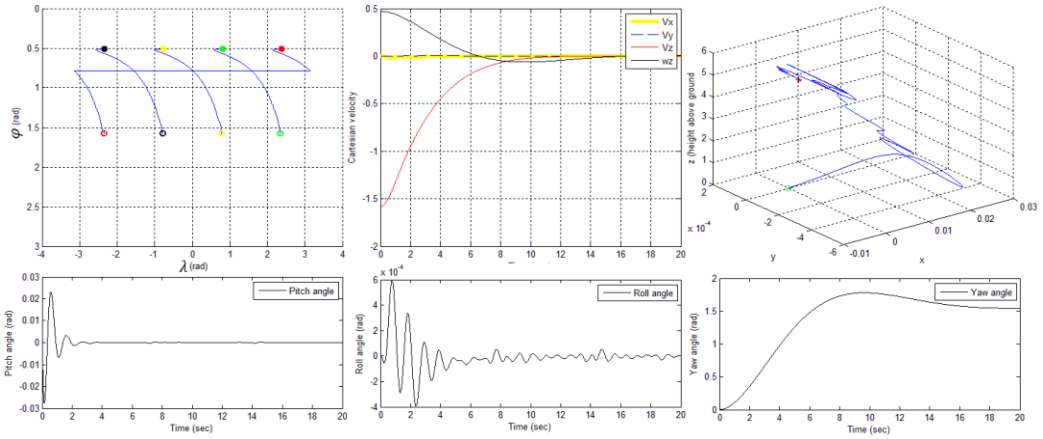

Figure 6 Case 3: a) The path of the point features in the $\lambda\varphi$ –space. "o" denotes initial position, "*" denotes the final position of features. b) Spatial velocity components. c) Vehicle/ camera position in Cartesian space. "o" denotes initial position, "*" denotes the final position of features. d) Attitude response for pitch, roll, and yaw angles. Note: Arrangement of figures is [a b c; d]

Table 1 Simulation parameters for vision system

Vision system parameters	
Number of target points	**4**
Position of target points $\boldsymbol{P} = (\boldsymbol{X}, \boldsymbol{Y}, \boldsymbol{Z})$	$\boldsymbol{P_1} = (-2, -2, 0)$ $\boldsymbol{P_2} = (-2, 2, 0)$ $\boldsymbol{P_3} = (2, 2, 0)$ $\boldsymbol{P_4} = (2, -2, 0)$
Desired position of the target points on the $\boldsymbol{\lambda\varphi}$ – space $\boldsymbol{p^*} = (\boldsymbol{\varphi^*}, \boldsymbol{\lambda^*})$	$\boldsymbol{p_1}^* = (0.5148, 2.3562)$ $\boldsymbol{p_2}^* = (0.5148, 0.7854)$ $\boldsymbol{p_3}^* = (0.5148, -0.7854)$ $\boldsymbol{p_4}^* = (0.5148, -2.3562)$
Gain $\boldsymbol{\alpha}$	0.3

Table 2 Flight controller parameters

Nominal velocity controller (Velocity loop)	
	$\boldsymbol{K_1^\phi = 0.1}$, $\boldsymbol{K_2^\phi = 2}$ $\boldsymbol{K_1^\theta = -0.1}$, $\boldsymbol{K_2^\theta = 2}$ $\boldsymbol{K_1^T = -40}$, $\boldsymbol{K_2^T = 1}$
Attitude controller (Attitude loop)	
Nominal attitude controller	$\boldsymbol{K_\theta^P = -400}$, $\boldsymbol{K_\theta^D = 0.1}$ $\boldsymbol{K_\phi^P = -400}$, $\boldsymbol{K_\phi^D = 0.1}$ $\boldsymbol{K_1^\psi = -100}$, $\boldsymbol{K_2^\psi = 1}$
Robust compensator	$\boldsymbol{f_{l\phi} = 5}$, $\boldsymbol{f_{s\phi} = 1}$ $\boldsymbol{f_{l\theta} = 5000}$, $\boldsymbol{f_{s\theta} = 100}$ $\boldsymbol{f_{l\psi} = 5}$, $\boldsymbol{f_{s\psi} = 1}$

4.3 Case 3: Hovering Mission With The Proposed Controller Under The Effects Of Multiple Uncertainties

In this case, the robust compensator is integrated into the existing attitude closed-loop system with parameters as presented in Table 2. As can be seen in Figure 6, the dynamical tracking performance of the closed-loop control system is extremely improved. The feature points have smooth trajectories in the $\lambda\varphi$ – space toward their desired position and the multirotor MAV successfully hovered above the target points in Cartesian space and almost held to its horizontal position. The robust compensating signal for pitch subsystem ${u_\theta}^{RC}$ successfully compensated the q_θ by sufficiently large parameters $f_{l\theta}$ and $f_{s\theta}$. If uncertainties are considered for roll and yaw subsystems, the behaviour is also similar with sufficiently large f_{li} and f_{si} $(i = \phi, \psi)$.

5.0 CONCLUSION

This paper proposes an image-based robust hovering control of the multirotor MAV which considers the effects of multiple uncertainties in angular dynamics of vehicle. The proposed method is robust against uncertainties which contain external disturbances, nonlinear dynamics, coupling, and parametric uncertainties and does not require keeping target features in the field of view. The simulation results proved the effectiveness and robustness of the proposed closed-loop system.

This research aims for real-time implementation which is a challenging task due to uncertainties in image dynamics.

Acknowledgement

This research was mainly supported by Malaysia-Japan International Institute of Technology, Universiti Teknologi Malaysia (UTM) and Ministry of Higher Education Malaysia under Research University Grant (vote no: 05H70).

References

[1] Hutchinson, S., Hager, G. and Cork, P. 1996. A Tutorial on Visual Servo Control. IEEE Trans. Robotics and Automation. (63): 651-670.

[2] Hamel, T. and Mahony, R. 2002. Visual Servoing of an Underactuated Dynamic Rigid-Body System an Image Based Approach. IEEE Trans. Robotics and Automation. (18): 187-198.

[3] Mejias, L., Saripalli, S., Campoy, P., and Sukhatme, G. 2006. Visual servoing of An Autonomous Helicopter in Urban Areas Using Feature Tracking. Journal of Field Robotics. 23(3-4): 185-199.

[4] Saripalli, S., Sukhatme, G. S., Mejias, L. O., Cervera, P. C. 2005. Detection and Tracking of External Features in an Urban Environment Using an Autonomous Helicopter. IEEE International Conference on Robotics and Automation. 3972-3977.

[5] Peliti, P., Rosa, L., Oriolo, G., and Vendittelli, M. 2012. Vision-based Loitering over a Target for a fixed-Wing UAV. 10th International IFAC Symposium on Robot Control. (): 51-57.

[6] Saunders, J. and Beard, R. 2008. Tracking a Target in Wind Using a Micro Air Vehicle with a fixed Angle Camera. American Control Conference. 3863-3868.

[7] Bourquardez, O. and Chaumette, F. 2007. Visual Servoing of an Airplane for Alignment with Respect to a Runway. IEEE International Conference on Robotics and Automation. 1330-1335.

[8] Coutard, L., Chaumette, F., and Pflimlin, J. –M. 2011. Automatic landing on aircraft carrier by visual servoing. IEEE/RSJ International Conference on Intelligent Robots and Systems. 2843-2848.

[9] Bourquardez O. and Chaumette, F. 2007. Visual Servoing of an Airplane for autolanding. IEEE/RSJ International Conference on Intelligent Robots and Systems. 1314-1319.

[10] Huh, S. and Shim, D. H. 2010. A Vision-based Automatic Landing Method for fixed-wing UAVs. Journal of Intelligent and Robotic Systems. 217-231.

[11] Serra, P., Bras, F. L., Hamel, T., Silvestre, C., and Cunha, R. 2010. Nonlinear IBVS Controller for the flare Maneuver of fixed-wing Aircraft Using Optical flow. 49th IEEE Conference on Decision and Control. 1656-1661.

[12] Zhong, Y. 2002. Robust Output Tracking Control of SISO Plants with Multiple Operating Points and with Parametric and Unstructured Uncertainties. Int. J. Control. 75: 219–241.

[13] Corke, P. . 2010. Spherical Image-based Visual Servo and Structure Estimation. IEEE Int. Conf. on Robotics and Automation. 5550-5555.

[14] Castillo, P., Dzul, A., and Lozano, R. 2004. Real-time Stabilization and Tracking of a Four-rotor Mini Rotorcraft. IEEE Transactions on Control Systems Technology. 12(4): 510–516.

[15] Pounds, P. 2007. Design, Construction, and Control of a Large Quadrotor Micro Air Vehicle. PhD thesis, Australian National University.

[16] Derawi, D., Salim, N. D., Zamzuri, H., Rahman, M. A. A., Nonami, K. 2016. Robust Attitude Control Design for a Low-cost Hexarotor Micro Aerial Vehicle (MAV). Transactions of the Institute of Measurement and Control.